Ultrafast Manipulation of Electron Spin Coherence

J. A. Gupta, *et al.*

Science **292**, 2458 (2001);
DOI: 10.1126/science.1061169

Science (print ISSN 0036-8075; online ISSN 1095-9203) is published weekly, except the last week in December, by the American Association for the Advancement of Science, 1200 New York Avenue NW, Washington, DC 20005.

and Plasma Sciences Society and the Institute of Electrical and Electronic Engineers, location, 1998), pp. 317–323.
47. E. N. Parker, in *Cosmic Winds and the Heliosphere*, J. R. Jokipii, C. P. Sonett, M. S. Giampapa, Eds. (Univ. of Arizona Press, Tucson, AZ, 1997), pp. 3–27.
48. E. J. Smith, in *The Sun in Time*, C. P. Sonett, M. S. Giampapa, M. S. Matthews, Eds. (Univ. of Arizona Press, Tucson, AZ, 1991), pp. 175–201.
49. P. Damon, C. P. Sonnet, in *The Sun in Time*, C. P. Sonnet, M. S. Giampapa, M. S. Matthews, Eds. (Univ. of Arizona Press, Tucson, AZ, 1991), pp. 360–388.
50. M. Stuiver, *J. Geophys. Res.* **66**, 273 (1961).
51. J. C. Houtermans, thesis, University of Bern, Bern, Switzerland (1971).
52. H. E. Suess, *Radiocarbon* **22**, 200 (1980).
53. K. O'Brien, A. D. L. Z. Lerner, M. A. Shea, D. F. Smart, in *The Sun in Time*, C. P. Sonnet, M. S. Giampapa, M. S. Matthews, Eds. (Univ. of Arizona Press, Tucson, AZ, 1991), pp. 317–343.
54. A 13-box carbon cycle model was used that included reservoirs for the atmosphere, terrestrial biosphere, soils, ocean sediments, and a 9-box ocean. Reservoir size and fluxes were brought to an initial balanced state in which both ^{12}C and ^{14}C concentrations reflected the modern prebomb pulse abundances (*45*, *55*, *56*). A globally averaged modern ^{14}C production rate of 2.03 atoms cm^{-2} s^{-1} was used (*42*), although this value is probably uncertain to about ±10% (*63*). The terrestrial magnetic field intensity dependence used (*42*) assumes a solar modulation parameter of ϕ = 550 equal to an average value for the period 1953–95, whereas the SINT200 (*57*) stacked paleomagnetic record was used as the record of terrestrial magnetic field intensity. The total active carbon reservoir size was set at 54,600 Pg of C, as required by a steady state ^{14}C production rate of 2.03 atoms cm^{-2} s^{-1} and the known modern ^{14}C activities in the various reservoirs (*55*). We define the active carbon reservoir as that carbon that may exchange with the atmosphere on 50-ka time scales. Because the production rate could only have been greater in the past 50 ka (because we are now at a geomagnetic maximum), the minimum size of the active carbon cycle is determined in the following way: If $(\partial N/\partial t)$ global = 2.03 atoms cm^{-2} s^{-1} × area of Earth, then the global ^{14}C inventory is given by $(\partial N/\partial t)$ global/λ_{14C} (global), and the inventory of ^{12}C is given by ^{14}C(global)/($^{14}C/^{12}C$)average = ^{12}C(active carbon cycle). Thus, ^{12}C(active carbon cycle) = 54,600 Pg of C. Because there are only 39,400 Pg of C (*45*) in the ocean + atmosphere + biosphere + active terrestrial soils, this means there are additionally about 15,200 Pg of C contained in other parts of the active carbon cycle. The only element of the active carbon cycle large enough to contain this amount of carbon is ocean carbonate sediments. If these sediments are formed in the ocean mixed layer, then the initial ($^{14}C/^{12}C$) must be the same as that of the mixed layer (i.e., FM = 0.85). This implies that at steady state the flux of carbon to this sedimentary sink must be on average 1.85 Pg of C $year^{-1}$.
55. W. S. Broecker, T.-H. Peng, *Tracers in the Sea* (Lamont-Doherty Geological Observatory, Palisades, NY, 1982).
56. G. Munhoven, thesis, Université de Liége, Liége, Belgium (1997).
57. Y. Guyodo, J.-P. Valet, *Earth Planet. Sci. Lett.* **143**, 23 (1996).
58. C. Laj, C. Kissel, A. Mazaud, J. E. T. Channel, J. Beer, *Philos. Trans. R. Soc. London* **358**, 1009 (2000).
59. C. Kissel *et al.*, *Earth Planet. Sci. Lett.* **171**, 489 (1999).
60. Most estimates of carbonate sedimentation rates for the modern world range between 0.24 and 2.0 Pg of C $year^{-1}$.
61. H. Heinrich, *Quat. Res.* **29**, 143 (1988).
62. P. E. Damon, R. E. Sternberg, *Radiocarbon* **31**, 697 (1989).
63. R. C. Finkel, K. Nishiizumi, *J. Geophys. Res.* **102**, 26699 (1997).
64. This paper is dedicated to the memory of R. Palmer and R. Parker, who died in separate diving incidents in 1997. We are extremely grateful to both of them for their invaluable contributions to exploration and fieldwork in the Blue Holes of the Bahamas.

17 October 2000; accepted 24 April 2001
Published online 11 May 2001;
10.1126/science.1056649
Include this information when citing this paper.

REPORTS

Ultrafast Manipulation of Electron Spin Coherence

J. A. Gupta,[1] R. Knobel,[2] N. Samarth,[2] D. D. Awschalom[1]*

A technique is developed with the potential for coherent all-optical control over electron spins in semiconductors on femtosecond time scales. The experiments show that optical "tipping" pulses can enact substantial rotations of electron spins through a mechanism dependent on the optical Stark effect. These rotations were measured as changes in the amplitude of spin precession after optical excitation in a transverse magnetic field and approach $\pi/2$ radians. A prototype sequence of two tipping pulses indicates that the rotation is reversible, a result that establishes the coherent nature of the tipping process.

Multiple pulse sequences in time-domain nuclear magnetic resonance and electron spin resonance (ESR) experiments are widely used to study spin-spin interactions and spin dephasing in inhomogeneous magnetic environments (*1*). A canonical sequence consists of a $\pi/2$ pulse to generate a nonequilibrium transverse spin polarization followed by a π-pulse that may enact a rephasing ("spin echo") of transverse spin if inhomogeneous broadening dominates the ensemble spin dynamics (*2*). Current technology limits the number of systems to which pulsed-ESR experiments can be applied because the minimum achievable pulse length of ~10 ns should be much smaller than the spin coherence time (*1*). To apply pulse sequences to study conduction-band electron spin dynamics in a variety of semiconductors where spin lifetimes can vary from ~3 ps (*3*) to ~130 ns (*4*), a complementary ESR technique capable of much shorter pulse widths is desirable. Application of spin echo sequences might be of particular interest in semiconductor quantum dots, where inhomogeneous broadening can limit spin lifetimes (*5*). Such a technique could also be useful for spin-based implementations of quantum computing in solid-state systems (*6*), where it is necessary to perform many operations ($>10^4$) on a quantum bit within the coherence time to realize full computation with error correction (*7*). The ability to perform spin operations on femtosecond time scales would satisfy this need in a number of semiconductor systems and may be applicable to single quantum bits using optical probes with high spatial resolution.

Here we present time-resolved Faraday rotation experiments that extend a technique first applied in atomic sodium (*8*) to semiconductor nanostructures by using ultrafast laser pulses to produce coherent rotations of electron spins (*9*). In our experiments, a pump pulse optically excites spin-polarized electrons that precess about a static magnetic field. A second below–band gap "tipping" pulse produces an additional effective magnetic field that can reach 20 T through the optical Stark effect (*10*). Effective field strengths are calculated from measurements of Stark shifts and depend on the pulse intensity, polarization, and energy. This field is used to coherently rotate electron spins by angles that approach $\pi/2$, as monitored through the Faraday rotation imparted to a probe pulse. A sequence of two tipping pulses suggests that spin coherence is preserved during the tipping process. Because the tipping pulses additionally excite a small number of real carriers, a variety of checks were performed to identify resultant background contributions. Although the tipping effects can be qualitatively interpreted as rotations about a light-induced effective field, quantitative comparisons of the tipping angle from Faraday rotation data with that expected from measured Stark shifts reveal a significant discrepancy.

Samples were chosen that illustrate a variety

[1]Department of Physics, University of California, Santa Barbara, CA 93106, USA. [2]Department of Physics, The Pennsylvania State University, University Park, PA 16802, USA.

*To whom correspondence should be addressed. E-mail: awsch@physics.ucsb.edu

of electronic and magnetic environments in which this technique can be applied. The samples consist of 10 150 Å–wide $Zn_{1-x}Cd_xSe$ ($x \sim 0.33$) quantum wells (QWs) fabricated with an all-digital approach that uses a short-period ZnSe/CdSe superlattice as the confining region (*11*). In addition to modulation-doped ($n = 4.1 \times 10^{11}$ cm^{-2}) and undoped QW samples, a magnetic QW was studied in which submonolayer MnSe planes were inserted into the confining region that increase the effective electron *g* factor (*3*). Synchronized optical parametric amplifiers (250-kHz repetition rate) produce two independently tunable (2.6 to 1.7eV) pump pulses and probe pulses of a white light continuum (each ~150 fs in duration) that were focused to a ~100-μm-diameter spot on the sample. The substrate was removed from a circular region of the sample, permitting measurements in transmission on free-standing epilayers.

First studied in atoms (*12*), the optical Stark effect in semiconductors has been explained as a repulsive interaction between real and virtual excitons that are created by probe and below–band gap pump photons, respectively (*13*). The end result is a shift ΔE, of the absorption spectrum toward higher energy that lasts for the duration of the pump-probe correlation time (typically 200 to 500 fs). ΔE is proportional to the pump intensity and inversely proportional to the pump detuning (*13*), in our case given by $\Delta \equiv E_{hh} - E_p$, where E_{hh} and E_p are the heavy-hole exciton and pump energies. Stark shifts in these QWs follow optical selection rules that govern the coupling of pump photons to heavy-hole (hh) and light-hole (lh) exciton transitions, visible as peaks in the linear absorption spectra (Fig. 1A). Illustrated in Fig. 1B, the solid lines show the conduction and valence band levels shifted from their unperturbed values (dotted lines) in the presence of a below–band gap, σ^+-polarized pump pulse (*14*). When tuned to the hh exciton absorption energy, co- or counterpolarized probe pulses (blue or red arrows in Fig. 1B) measure shifts of σ^+ or σ^- hh excitons. The σ^+ hh exciton shift reflects coupling of pump photons to the σ^+ hh exciton, whereas the σ^- hh exciton shift arises indirectly through the shift of the $\langle +1/2|$ conduction band level produced by coupling of the pump to the σ^+ lh exciton. Because of both optical selection rules and larger pump detuning from the lh exciton energy, the σ^- hh exciton shift is smaller (*14*).

Shifts were measured as pump-induced changes in the absorption spectrum given by $\Delta\alpha L \equiv (\alpha_0 - \alpha)L$, where α_0 is the absorption coefficient without the pump, α is the coefficient with the pump as measured by a time-delayed probe, and L is the sample thickness. In these initial two-beam experiments, the pump and probe were both circularly polarized with Soleil-Babinet compensators, and the probe was spectrally resolved and detected at an energy E_d (*15*). Absolute values of the Stark shift were calculated from the relation $\Delta E = (\Delta\alpha L)(d\alpha L/dE)^{-1}$ (*15*).

Figure 1C shows the pump-intensity dependence of Stark shifts for co- and counterpolarized probe pulses (ΔE_{co} and $\Delta E_{counter}$) taken at two values of detuning for the undoped QW sample. There is a departure from linearity at higher intensity that is consistent with previous studies (*15*), in addition to the expected increase in shift as the pump detuning is reduced. The data are indicative of a net conduction-band spin splitting given by $\delta_{CB} = 1/2\Delta E_{co} - \Delta E_{counter}$ (*14*) that may be described as an effective magnetic field along the laser direction, $\vec{H}_{Stark} = \delta_{CB}/(g_e\mu_B)\hat{x}$, where $g_e = 1.1$ is the electron *g* factor in this sample. This field is plotted versus intensity in Fig. 1D where a plateau value of ~19 T ($\delta_{CB} = 1.2$ meV) with $\Delta = 64$ meV results from a change in the relative intensity dependence of ΔE_{co} and $\Delta E_{counter}$ at high intensity. The ratio $\Delta E_{co}/\Delta E_{counter}$ can be compared with the theoretical expectation of ~6.5 calculated with measured values of hh and lh exciton energies (*14*). Data at higher detuning and low intensity agree with this value; differences with lower detuning and higher intensity may indicate a transition to a nonperturbative regime for which the theory is inappropriate.

In order to clearly observe the Stark shift, the pump energy must be adjusted to minimize the excitation of real carriers. Figure 1E shows that when the pump energy is higher than the hh exciton ($\Delta < 0$), real-carrier generation results in state-filling effects that

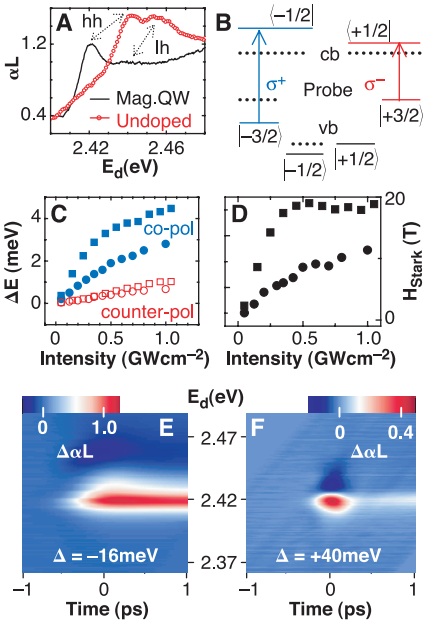

Fig. 1. (**A**) Absorption spectra for undoped (T = 10 K) and magnetic (T = 6 K) QWs. (**B**) Stark shifts arising from σ^+-polarized below–band gap pump pulses, measured by co- (σ^+) and counterpolarized (σ^-) probe pulses. (**C**) Dependence of Stark shifts on pump intensity, I_p, at T = 10 K for the undoped QW sample. The relative probe helicity is co- (blue symbols) and counterpolarized (red symbols) for detuning of Δ = 90 meV (circles) and Δ = 64 meV (squares). (**D**) Effective magnetic field calculated from the data in (C). (**E** and **F**) Spectrally resolved pump-induced changes in absorption ($\Delta\alpha L$) for the magnetic QW at T = 6 K (copolarized probe). (E) $\Delta = -16$ meV and I_p = 0.25 GW cm^{-2}. (F) $\Delta = +40$ meV and I_p = 1.0 GW cm^{-2}.

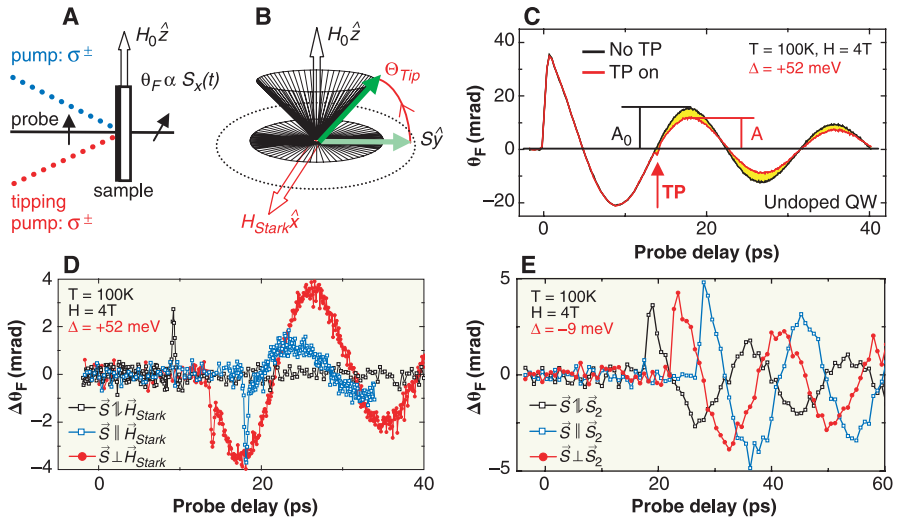

Fig. 2. (**A**) Experimental schematic. (**B**) $\vec{H}_{Stark}$ rotates $\vec{S}$ away from the *x*-*y* plane when $\vec{\tau} \neq 0$. (**C**) Data from the undoped QW showing amplitude reduction caused by the tipping pump. Data were taken with I_p = 25 MW cm^{-2}, E_p = 2.431 eV, E_d = 2.422 eV, E_{TP} = 2.375 eV (Δ = +52 meV), and I_{TP} = 0.5 GW cm^{-2}. (**D** and **E**) Comparison of the difference signal $\Delta\theta_F = \theta_F^{TPon} - \theta_F^{noTP}$ with the TP positioned such that $\vec{H}_{stark}$ (D) or $\vec{S}_2$ (E) is parallel, perpendicular, or antiparallel to $\vec{S}$. (D) Same parameters as (C). The sharp spike in each scan marks the arrival of the TP. (E) $\Delta = -9$ meV and I_{TP} = 12.5 MW cm^{-2}.

bleach the QW absorption, visible as a red "streak" that persists for the carrier recombination time (>100 ps, not shown in figure). When the pump energy is tuned below the band gap ($\Delta > 0$), the generation of real carriers is energetically unfavorable, and a ~250-fs-wide feature appears in Fig. 1F that corresponds to a 5.1-meV shift. The lobed spectral shape reflects the change in sign of $d\alpha L/dE$ that occurs when the detection energy is scanned across the hh exciton peak. Tipping pump energies in the following experiments were chosen that represented a compromise between state-filling effects and magnitude of the Stark shift.

In time-resolved Faraday rotation experiments (Fig. 2A), a circularly polarized pump pulse (with $\Delta \sim 0$) excites spin-polarized electrons and holes along $\hat{x}$, perpendicular to an applied magnetic field $H_0\hat{z}$. Previous studies indicated that hole spins are either pinned along the QW growth direction or dephase rapidly (*3*). As a result, the Faraday rotation, θ_F, of linearly polarized probe pulses is proportional to $S_x(t)$, the projection of electron spin $\vec{S}$ on $\hat{x}$. Because the electron spins comprise a coherent superposition of eigenstates quantized by the field, θ_F oscillates as a function of probe delay at the Larmor spin precession frequency $\nu_L = g_e\mu_B H_0$. A circularly polarized tipping pump (TP) pulse (usually with $\Delta > 0$) was incident on the sample after the pump. The relative time delays of the three pulses incident on the sample could be independently adjusted with ~10-fs resolution, and data were collected by scanning either the probe or tipping pump delay. The three optical beams were modulated at different kHz-scale frequencies, and lock-in amplifiers were used to record changes in the total Faraday rotation induced by the pump and tipping pump pulses. This scheme was necessary for separately identifying signals initiated by the pump and TP alone, as well as signals due to their interaction. Data shown here were taken with reference to the pump modulation frequency to focus on dynamics of the spin magnetization excited by the pump.

Figure 2B depicts the rotation of spin polarization away from the *x*-*y* plane caused by the TP. The torque exerted by the TP is given by $\vec{\tau} = g_e\mu_B\vec{S} \times \vec{H}_{Stark}$ and is largest when $\vec{S}(t) \perp \vec{H}_{Stark}$, a situation that occurs whenever $\theta_F(t)$ crosses zero. Spin precession after the tipping event describes a cone about H_0; because θ_F only measures S_x, the amplitude is reduced. This is realized in Fig. 2C, where spin precession in the undoped QW is shown with the TP position indicated by the arrow. A priori, the tipping angle Θ_{tip} can be simply calculated from the relation $\Theta_{tip} = \mathrm{ArcCos}(A/A_0)$, where A and A_0 are the reduced and unperturbed amplitudes as shown in Fig. 2C.

However, the undesirable excitation of a small number of real carriers by the TP (~100 times fewer than the pump) complicates this analysis. Some real-carrier excitation was observed for the entire range of detuning studied (up to $\Delta = 120$ meV) and appears as a faint white streak in Fig. 1F. No net improvement was observed by increasing Δ, because both tipping effects and real-carrier generation were comparably reduced. Although energetically unfavorable, absorption of TP photons may occur because of low-energy states in the QW (perhaps related to impurity sites) (*16*) or phonon-assisted absorption (*17*); two-photon processes are unlikely because of the preservation of spin polarization and the dependence on detuning (not shown in figure). Because the lock-in detection scheme is "bidirectional," the signal detected at the pump modulation frequency can reflect both (i) TP-induced changes in θ_F from electron spins excited by the pump (the desired signal) and (ii) pump-induced changes in θ_F from electron spin excited by the TP (due to undesired real-carrier generation). The latter are detected because the TP excites fewer carriers when preceded by the pump than if the pump were absent, a change that is picked up in lock-in measurements at the pump modulation frequency as an added background. This background contribution to the measured signal does not reflect a change in the dynamics of the pump-excited spins but is merely superimposed on the desired tipping results. These state-filling effects are strongest when the spins excited by the pump and TP are parallel but generally exist to some degree at any relative polarization.

To study the consequences of these effects, Fig. 2D shows the signal $\Delta\theta_F = \theta_F^{TPon} - \theta_F^{noTP}$ corresponding to the difference between red and black curves in Fig. 2C with the TP (polarized so $\vec{H}_{Stark} \parallel \hat{x}$) positioned at three different points in the spin precession cycle. As expected, the difference signal is largest when the TP is positioned where $\vec{S}$ is perpendicular to $\vec{H}_{Stark}$ (red circles in Fig. 2D). State-filling effects result in the nonzero difference signal when $\vec{S}$ is parallel to $\vec{H}_{Stark}$ (blue squares) and are largely absent when $\vec{S}$ is antiparallel to $\vec{H}_{Stark}$ (black squares). To identify the optical Stark effect as the underlying mechanism for spin rotation, we did the same comparison with the TP energy chosen to excite an additional spin population $\vec{S}_2 \parallel -\hat{x}$ directly ($\Delta < 0$). State-filling effects are dominant for this situation, so that $\Delta\theta_F$ is expected to be largest when $\vec{S}(t)$ is parallel to $\vec{S}_2$. Figure 2E shows that the magnitude of $\Delta\theta_F$ becomes progressively larger as the TP is moved from a position where $\vec{S}$ and $\vec{S}_2$ are antiparallel to a position where $\vec{S}$ and $\vec{S}_2$ are parallel. The phase differences present in the oscillations of $\Delta\theta_F$ reflect the initial time and polarization of spins excited by the TP relative to those previously excited by the pump.

Figure 3 summarizes an effort for the magnetic QW to subtract real-carrier background contributions from the calculated value of Θ_{tip} by studying the dependence of the tipping angle on TP intensity. Spin precession in this sample is indicative of an enhanced effective g factor (g_e ~20) and decreased spin lifetime characteristic of QWs with a large exchange interaction between electron spins and paramagnetic Mn^{2+} ions (*3*). The reduction in amplitude caused by the TP ($\vec{H}_{Stark} \parallel \hat{x}$, $\Delta = 46$ meV) increases with TP intensity (Fig. 3A), eventually causing a reversal in sign (heavy solid curve) that in the absence of state-filling effects would indicate a tipping angle greater than $\pi/2$. To quantify contributions from state-filling effects, we

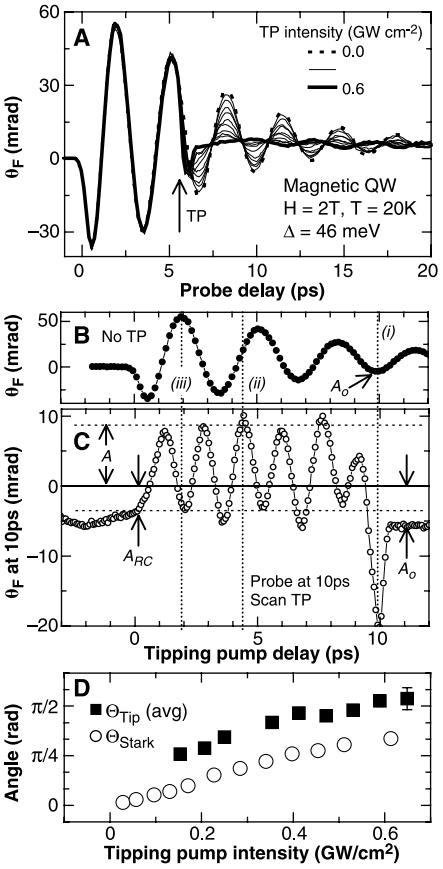

Fig. 3. (**A**) Intensity dependence of tipping effects in the magnetic QW at $T = 20$ K, $H = 2$ T with $E_p = 2.446$ eV, $I_p = 10$ MW cm^{-2}, $E_d = 2.410$ eV, and $\Delta = 46$ meV. (**B**) θ_F versus probe delay without TP. Dotted line *i* indicates the peak amplitude monitored in (C). The time base was slightly adjusted for clarity. (**C**) Data with probe at 10 ps and scanning TP delay. Peaks in the scan occur when $\vec{H}_{Stark}$ is perpendicular to $\vec{S}(\Delta t_{TP})$ (e.g., dotted line *ii*), whereas valleys occur when $\vec{H}_{Stark}$ and $\vec{S}(\Delta t_{TP})$ are parallel (*iii*) or antiparallel. $I_{TP} = 0.5$ GW cm^{-2}. (**D**) Comparison of expected (Θ_{Stark}) and measured (Θ_{tip}) rotation angles calculated from Stark shifts and Faraday rotation data.

took data by fixing the probe time delay at a peak in the spin precession cycle [dotted line *i* in Fig. 3, B and C, with $\vec{S}(10\ \mathrm{ps})\|-\hat{x}$] and monitoring the change in amplitude as a function of TP time delay, Δt_{TP}. Figure 3B shows spin precession data taken in the absence of the TP, included as a reference. Peaks in the signal detected at 10 ps (Fig. 3C) occur when $\vec{S}(\Delta t_{TP})\perp\vec{H}_{Stark}$ (for example, dotted line *ii*). Consistent with Fig. 2, D and E, the amplitude does not return to its unperturbed value A_0 when $\vec{S}(\Delta t_{TP})\|\vec{H}_{Stark}$ (dotted line *iii*) because of state-filling effects. These situations appear as valleys in Fig. 3C that are closer to A_0 when $\vec{S}(\Delta t_{TP})$ and $\vec{H}_{Stark}$ are antiparallel than when they are parallel. The valley at $\Delta t_{TP} = 10$ ps is associated with the Stark shift itself and marks the point where probe and TP overlap in time.

To calculate Θ_{tip}, we recorded the extrema in Fig. 3C, yielding values of A_{RC} and A, where A_{RC} is a measure of the background contribution due to real-carrier effects. Because only real-carrier effects are present at the valleys in Fig. 3C, we subtract this contribution to Θ_{tip} using the relation $\Theta_{tip} = \mathrm{ArcCos}\{[A - (A_{RC} - A_0)]/A_0\}$ (*18*). Figure 3D compares the results from this calculation averaged over all peaks and valleys from $0 < \Delta t_{TP} < 9$ ps in Fig. 3C with values for Θ_{tip} expected from Stark shift data:

$$\Theta_{Stark} = \frac{1}{\hbar}\int_{-\infty}^{+\infty}\delta_{CB}(t)\mathrm{d}t,$$

where $\hbar$ is Planck's constant divided by 2π. Here the conduction-band spin splitting is integrated over the temporal profile of the TP (Gaussian with a width of ~400 fs). Although the two plots have a similar functional dependence on intensity, there is a significant discrepancy in magnitude. Earlier studies of hole spin dynamics have shown that in-plane magnetic fields can modify optical selection rules because of valence-band mixing (*3*, *19*). Although we do not observe much change in the Stark shift with magnetic field, it may be that the relative valence and conduction-band contributions to the shift change with field, effectively causing an increase in δ_{CB}. It is perhaps more likely that the simple calculations presented here are inadequate for describing the highly nonadiabatic, impulsive effects of these below–band gap tipping pulses.

In addition to possible systematic errors not accounted for in the subtraction routine above, the difference between expected and measured tipping angles could be due to an incoherent reduction in amplitude caused by the tipping process itself. We investigated this possibility by further extending the technique to include two tipping pumps (TP1 and TP2), to establish the reversibility and coherent nature of the tipping process (*20*). To begin with, TP1 arrives at a zero crossing in θ_F (t) ($\vec{S}\perp\vec{H}_{TP1}$), causing spins to be tipped away from the x-y plane and resulting in a reduction of amplitude as before (Fig. 4B). The spins then are allowed to precess a half-cycle before they are tipped again by TP2, resulting in a second torque of opposite sign for copolarized TPs (Fig. 4C) and of the same sign for counterpolarized TPs (Fig. 4A). The data in Fig. 4D were taken with equal-intensity TPs and show a reversal or enhancement of the net tipping angle as the TP2 helicity is varied, indicating that spin coherence is largely preserved during the tipping process. Data were taken with various combinations of relative circular and linear polarizations to verify that the dependence on TP2 helicity existed only when preceded by a circularly polarized TP1. Figure 4E shows one such check, where data taken without TP1 show a similar amplitude reduction for the two TP2 helicities (*21*).

We expect that spin echoes could occur for imperfect tipping pulses if $\pi/2 < \Theta_{tip} < \pi$. Because the echo amplitude should sinusoidally increase as the tipping angle approaches π, the current degree of rotation is just at the limit where echoes may start to become observable. However, an additional requirement for echo observation is that inhomogeneous dephasing in the sample limits the spin lifetime. Although this condition was not clearly met in the present samples, model systems may be realized by specifically engineering inhomogeneous dephasing into magnetic heterostructures based on the one studied here. In conclusion, these experiments demonstrate a principle by which π-pulses may be constructed to coherently control spins in semiconductors on femtosecond time scales.

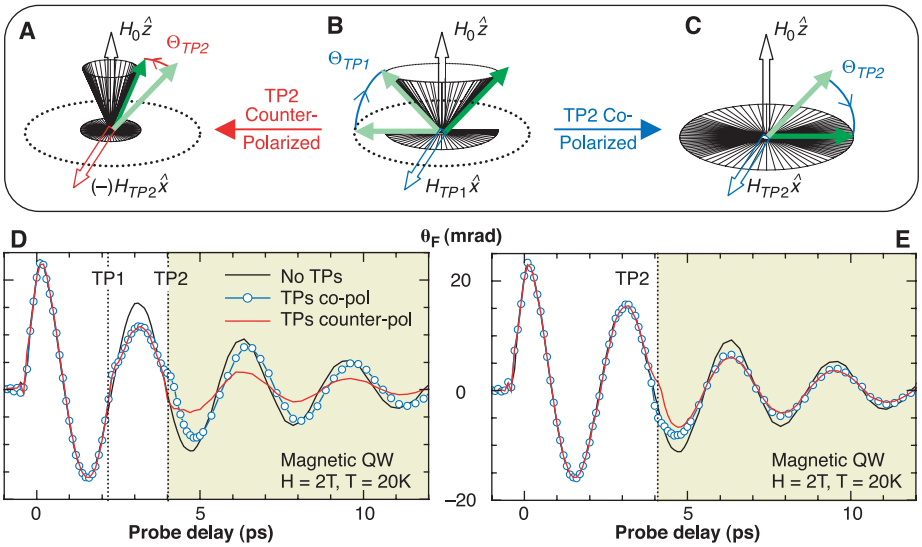

Fig. 4. (**A** to **C**) Illustration of the net tipping angle with two co- and counterpolarized tipping pumps. Parameters for the tipping pumps in (**D** and **E**): Δ = 51 meV, I_{TP} = 0.2 GW cm^{-2}. (D) Data taken with tipping pumps positioned at consecutive zero crossings, comparing the situations in (A) (red) and (C) (blue). (E) The dependence of the net tipping angle on TP2 helicity vanishes in the absence of TP1.

References and Notes

1. A. Abragam, *The Principles of Nuclear Magnetism* (Clarendon Press, Oxford, 1961).
2. E. Hahn, *Phys. Rev.* **80**, 580 (1950).
3. S. A. Crooker, D. D. Awschalom, J. J. Baumberg, F. Flack, N. Samarth, *Phys. Rev. B* **56**, 7574 (1997).
4. J. M. Kikkawa, D. D. Awschalom, *Phys. Rev. Lett.* **80**, 4313 (1998).
5. J. A. Gupta, D. D. Awschalom, X. Peng, A. P. Alivisatos, *Phys. Rev. B* **59**, 10421 (1999).
6. D. Loss, D. P. DiVincenzo, *Phys. Rev. A* **57**, 120 (1998).
7. J. Preskill, http://xxx.lanl.gov/abs/quant-ph/9712048 (1997).
8. D. Suter, H. Klepel, J. Mlynek, *Phys. Rev. Lett.* **67**, 2001 (1991); M. Rosatzin, D. Suter, J. Mlynek, *Phys. Rev. A* **42**, 1839 (1990).
9. S. A. Crooker, thesis, University of California, Santa Barbara (1996).
10. C. Cohen-Tannoudji, J. Dupont-Roc, *Phys. Rev. A* **5**, 968 (1972).
11. O. Ray *et al.*, *Appl. Phys. Lett.* **76**, 1167 (2000).
12. C. Cohen Tannoudji, S. Reynaud, *J. Phys. B* **10**, 345 (1977).
13. M. Combescot, R. Combescot, *Phys. Rev. Lett.* **61**, 117 (1988).
14. M. Joffre, D. Hulin, A. Migus, M. Combescot, *Phys. Rev. Lett.* **62**, 74 (1989).
15. J. A. Gupta, D. D. Awschalom, *Phys. Rev. B* **63**, 085303 (2001).
16. O. Ray, I. P. Smorchkova, N. Samarth, *Phys. Rev. B* **59**, 9810 (1999).
17. A. Von Lehmen, J. E. Zucker, J. P. Heritage, D. S. Chemla, *Phys. Rev. B* **35**, 6479 (1987).
18. An offset (7 mrad) was subtracted from the signal so that the oscillations in θ_F were about zero for the calculations. This offset was likely an artifact due to the sample not being perfectly normal to the laser, thus resulting in a nonprecessing component of $\vec{S}$ along H_0.
19. T. Z. Kachlishvili, *Solid State Commun.* **80**, 283 (1991).
20. H. Mabuchi, personal communication.
21. In studies of the undoped and doped QW samples with a single TP, it was found that the reduction in amplitude was different for the two TP helicities, an effect that remains an open question.

22. We acknowledge the help of J. J. Berry and M. Poggio and support from the Defense Advanced Research Projects Agency/Office of Naval Research and the U.S Army Research Office.

29 March 2001; accepted 15 May 2001